Nano Research
2021, 14(1): 157–164
ISSN 1998-0124 CN 11-5974/O4
https://doi.org/10.1007/s12274-020-3060-x

Research Article

Multiple radial phosphorus segregations in GaAsP core–shell nanowires

H. Aruni Fonseka[1] (✉), Yunyan Zhang[2], James A. Gott[1], Richard Beanland[1], Huiyun Liu[2], and Ana M. Sanchez[1]

[1] *Department of Physics, University of Warwick, Coventry CV4 7AL, UK*
[2] *Department of Electronic and Electrical Engineering, University College London, London WC1E 7JE, UK*

Received: 9 July 2020 / **Revised:** 13 August 2020 / **Accepted:** 14 August 2020

ABSTRACT

Highly faceted geometries such as nanowires are prone to form self-formed features, especially those that are driven by segregation. Understanding these features is important in preventing their formation, understanding their effects on nanowire properties, or engineering them for applications. Single elemental segregation lines that run along the radii of the hexagonal cross-section have been a common observation in alloy semiconductor nanowires. Here, in GaAsP nanowires, two additional P rich bands are formed on either side of the primary band, resulting in a total of three segregation bands in the vicinity of three of the alternating radii. These bands are less intense than the primary band and their formation can be attributed to the inclined nanofacets that form in the vicinity of the vertices. The formation of the secondary bands requires a higher composition of P in the shell, and to be grown under conditions that increase the diffusivity difference between As and P. Furthermore, it is observed that the primary band can split into two narrow and parallel bands. This can take place in all six radii, making the cross sections to have up to a maximum of 18 radial segregation bands. With controlled growth, these features could be exploited to assemble multiple different quantum structures in a new dimension (circumferential direction) within nanowires.

KEYWORDS

compound semiconductor alloys, radial segregations, three-fold symmetry, surface chemical potential

1 Introduction

Epitaxial growth may deviate from its simple form due to growth rate anisotropy, strain, entropy of mixing in alloys and capillarity, forming unintended self-formed features [1, 2]. Nanowires, which themselves are a result of growth rate anisotropy, are particularly prone to develop such self-formed features due to coexistence of multiple growth facets. Different types of such nanowire features have been reported, including unintentional core–shell structures [3, 4], radial elemental segregations [5–12], alloy fluctuations [13, 14], longitudinal wires that form along the vertical edges [15–17] and pyramidical elemental segregations [18, 19]. Most of these exhibit optical properties consistent with self-formed passivation layers [3] or quantum structures such as quantum dots [13, 18, 19], wires [15, 16], and rings [20, 21]. While some of these could be detrimental by giving rise to unintentional emission or acting as carrier traps, others such as the pyramidical elemental segregations have been reported to show superior optical properties, far exceeding that of those that are intentionally grown [18, 19]. On the other hand, self-assembly has long been used as a means of assembling structures in the nanoscale with a level of precision and ease that may not otherwise have been possible, and same has been true in relation to nanowires [16, 18, 19, 22].

These self-formations can be treated in three ways. Firstly, avoiding their formation (in cases that they are detrimental) [13, 14], secondly using them as competitive alternatives for intentional structures [3, 15] or in a third way by exploiting them as a basis to form novel device architectures through controlled and engineered growth, such as by coupling with intentional structures, or self-assembly [23, 24]. However, in all three cases, it is important to understand the form, growth, and evolution of these self-formed features.

This work presents the formation of multiple radial segregation bands at the radii in high P containing ternary GaAsP nanowire shells. This observation is in contrast to the commonly observed six single bands that run along the radius following the corners of the hexagonal cross-section in shells of alloy materials [5–10, 12].Two prominent secondary bands are shown to form in the vicinity of the three radii in the <112> A direction. In addition to that, it is shown that the central P rich band can also be split into two narrow sub-bands in all radii, making the maximum possible total number of radial lines 18. To the best of our knowledge, such radial features have not been demonstrated before.

To date in nanowires, structures have only been stacked either in the axial or radial direction due to the layer by layer nature of epitaxial growth. This has led to the utilisation of only two of the available dimensions on nanowires, while the circumferential direction is left unexploited. In this work, the formation, evolution, compositions, and growth conditions required for the formation of these features are understood using principals of vapour-solid (VS) growth on non-planar

Address correspondence to a.fonseka.1@warwick.ac.uk

surfaces. This knowledge can be used to engineer the regions between the P rich bands to form quantum wells (QWs) along the circumference; a new form of nanowire based quantum structure, that may bear important implications for novel quantum device engineering [23, 24].

2 Results and discussion

2.1 Multiple radial segregations

Figure 1(a) shows an annular dark field (ADF) scanning transmission electron microscope (STEM) cross-section image from a $GaAs_{(1-x)}P_x$–$GaAs_{(1-y)}P_y$ core–shell nanowire with high (x, y > ~0.5) P compositions. Ga droplet self-catalysed GaAsP core and two GaAsP shells, with the outer layer identified by the higher level of alloy fluctuations [14] (striations) are demarcated by broken lines. The first (inner) shell is grown unintentionally during the Ga catalyst droplet consumption step, which took place at a higher temperature of 640 °C following the core growth. The second intentional shell was grown at a lower temperature of 550 °C. Further details pertaining to growth can be found in the experimental section and a scanning electron microscopy (SEM) image of the nanowires is shown in Fig. S1 in the Electronic Supplementary Material (ESM).

Dark bands that extend radially towards the corners of the hexagon are visible in both shells. These lines correspond to P rich bands as the contrast in ADF images is related to the atomic number, with lighter elements appearing in dark contrast. The fast fourier transform (FFT) of the image shown in the inset of Fig. 1(b) confirms that the nanowires facets are of {110} type, meaning that the radial lines are in the <112> directions. The vertices have a higher surface chemical potential due to its higher curvature that results from small width of {112} facets [1, 2, 8] (see Fig. S2 in the ESM). The formation of the P rich bands is due to As atoms that have higher mobility diffusing away from the high potential vertices better than the less mobile P atoms [1, 2, 6, 25]. Similar segregations that take place as single-bands along the nanowire radii are commonly observed for most III-V semiconductor alloys [5–10, 12, 26]. Note that the jaggedness of these lines in the current sample is due to the non-uniform cross sectional shape evolution of the nanowire, which means that the irregular hexagonal shape has been shifting during growth. Out of the six bands in the outer shell, three alternating ones are clearly darker and more prominent than the other three.

These nanowires have zincblende (ZB) crystal structure and the polarity arising from the existence of two types of atoms (anions and cations) within the crystal separates the six <112> directions into two (labelled A and B) polarities making the symmetry three-fold. The same type of facet can have different properties depending on its polarity, making the growth, diffusion, and decomposition different. This has been shown to cause the radial segregations in alloy III-V nanowires to have different sharpnesses and thicknesses between the radial lines present along the alternating <112> A and <112> B directions [6, 7]. Previous studies have shown that in GaAsP nanowire shells the darker P rich bands form at the <112> A radii due to the relatively weaker bond that group V materials form on predominantly Ga terminated A polar {112} surfaces [6, 15]. The relative directions ascertained accordingly are marked in Fig. 1(a).

Figure 1(b) is a higher magnification image of the same cross-section. The image is falsely colourised in order to enhance contrast and highlight features. A closer inspection reveals that instead of one, three P rich bands coexist in two of the <112> A radii (α and γ) of the inner shell. This is further verified by the respective integrated intensity profiles shown inset. The middle band (henceforth referred to as primary band) is darker than those on the two sides (secondary bands). The third

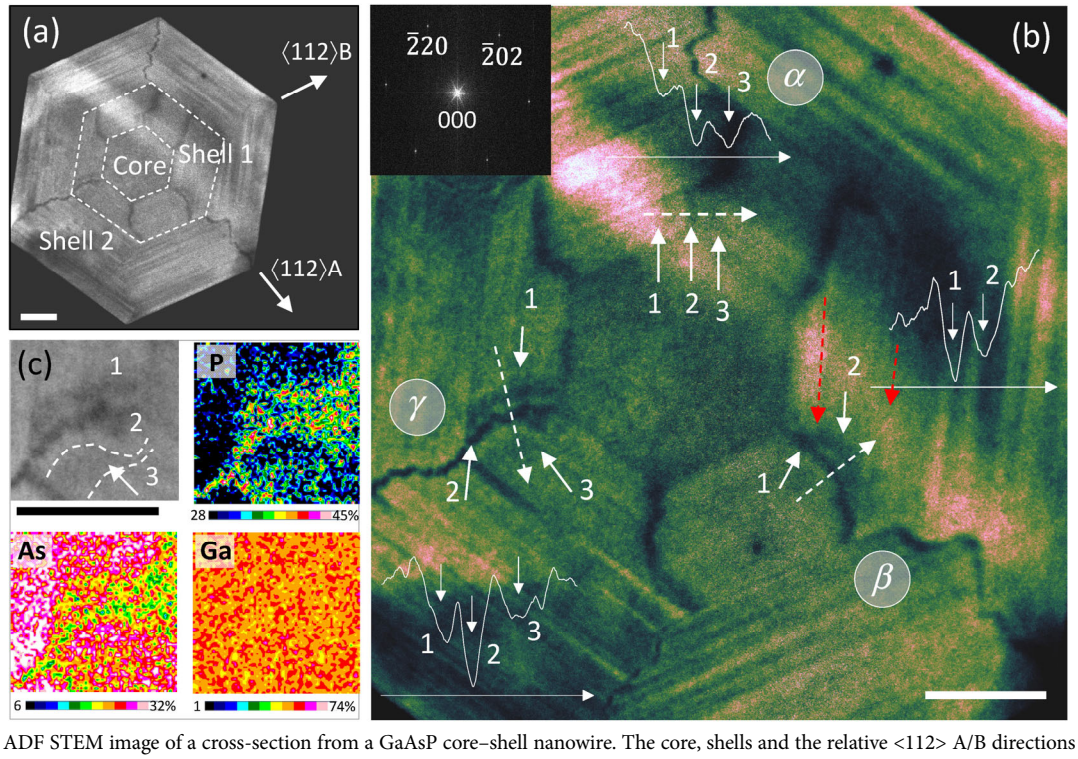

Figure 1 (a) ADF STEM image of a cross-section from a GaAsP core–shell nanowire. The core, shells and the relative <112> A/B directions are indicated. (b) False colour higher magnification image of (a), showing the core and first shell. Numbered white solid arrows indicate multiple radial P-rich bands formed at <112> A radii. The inset plots show the integrated intensity profiles from a 2.5 nm wide strip around the respective white broken arrow. The dips in these intensity profiles correspond to the P rich bands. The inset FFT confirms the {110} type nanowire facets. (c) EDX maps showing P, As and Ga elemental distribution at the radius γ in shell 1. All scale bars are 20 nm and the colour scales in (c) are linear between the respective indicated values.

radius (β) of the same polarity has two lines, the primary and one secondary. Their P rich nature is further verified by the EDX measurements and relevant elemental maps of radius γ is shown in Fig. 1(c). The alternative three <112> B radii consist of typical single P rich bands.

The secondary radial bands seen in <112> A radii appears to be sensitive to the compositional fluctuations (which could vary up to ~ 15% of P in shell 1); with both in α and the one in β terminating at alloy fluctuations. Furthermore, the secondary band in β only appears within a P rich region (indicated by the red arrows) within the alloy fluctuation. These observations suggest that the secondary radial bands are highly sensitive to the composition. Another important observation is that the secondary bands are not continued to the outer shell which has a similar or slightly higher average P composition. While the high level of alloy fluctuations (which could vary up to ~ 30% of P composition in shell 2) could be one strong reason, this observation also indicates that growth parameters could also affect the secondary band formation. The effect of composition and growth parameters will be discussed in detail later.

Not all nanowires in this sample showed secondary P bands, or other features that are discussed later, most likely due to their high sensitivity to composition and growth rate, which slightly varied between these randomly positioned nanowires. Combinations of one or both secondary lines forming in one, two or all three <112> A radii were observed in others. One such example can be seen in Fig. 4.

2.2 Nano-facet formation at the alternating vertices

In order to investigate the origin of these multiple radial lines, a GaAsP core-only sample was grown using the same growth parameters as those used for the core of the above core–shell nanowires. Figure 2(a) shows ADF STEM image of a nanowire cross-section from this sample. As expected, the major side facets of these nanowire core were also of {110} type. However, in some nanowires, one or more of the alternative vertices deviate from the {110} facets, to form a slightly sharper vertex with a smaller angle than the typical 120°, as shown by the yellow broken guideline drawn parallel to the facets. Additional inclined nanofacets seem to exist on these alternating vertices as indicated by the red arrows in the same image. These facets would most likely have formed during limited VS radial growth that took place during nanowire core growth.

A recent report demonstrated formation of similar nanofacets at the alternating vertices of AlAs nanowire shells which made them deviate from the regular hexagonal cross-section and form sharper vertices [26]. Another report [27] has successfully simulated this growth and shown that the formation of nano-facets is a combinational effect of surface energy anisotropy, orientation-dependent growth rates (which is enhanced in the <112> B directions for AlAs) and extremely low surface mobility of AlAs. However, the selection of polarity, is still unclear. Hence, a mechanism based on facet polarity is proposed here.

At the vertices, the adatoms diffuse away from {112} facets to the adjacent {110} facets due to the higher surface potential of the former [1, 2]. If the diffusion length of the adatoms are limited, they would incorporate close to the respective corner of the receiving facet as shown in Fig. 2(b), and result in an evolution of new nanofacets slightly inclined to the {110} facets [28].

Polarity of the formed facets affects this process, leading to the observed 3-fold symmetry. The new inclined facets that are inclined inwards compared to the {110} facets will have opposite polarity to the respective {112} facet. For example, as

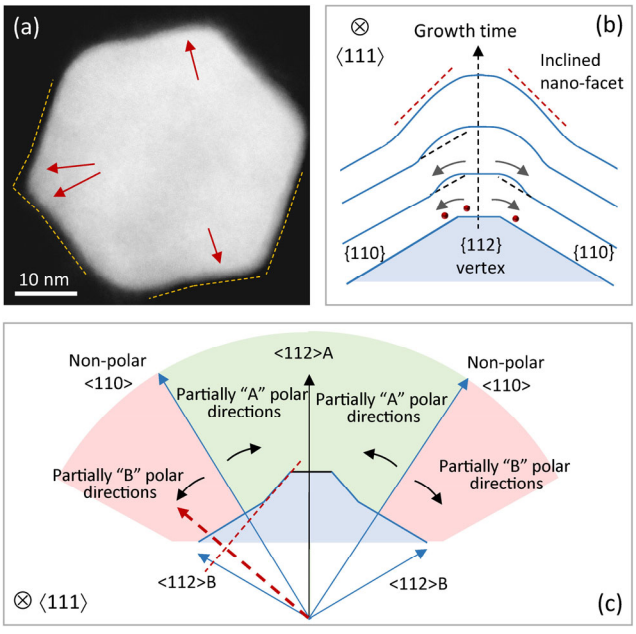

Figure 2 (a) ADF STEM image of a cross-section from a GaAsP core-only nanowire grown with the same growth conditions as the core of that shown in Fig. 1. Red arrows indicate the inclined facets formed at three of the alternating vertices and the yellow broken line is a guide to show the change in cross-sectional shape. (b) Schematic showing the proposed mechanism of inclined facet formation at the vertices. (c) Polarity of facets in the vicinity of vertices. Angles between facets are exaggerated for clarity. Inclined facets formed at a <112> A vertex will be of B polarity as shown by the red broken line and arrow.

shown in Fig. 2(c), those adjacent to {112} A facet, will have opposite, B type polarity. Polar surfaces can have inequal densities of group III and V atoms in the surface unit cell, as on {112} surfaces which show a ratio of 1:2 between the two groups, or be stoichiometric where the number of atoms of the two groups are equal, yet with a dissimilar bonding arrangement in the two types leading to an electrically charged surface [29–32]. In the latter case, the effect of polarity is much weaker. However, in either case, on B polar surfaces, group V atoms form stronger bonds with higher coordination numbers and vice-versa [6, 29–32] (see Section S1 in the ESM for some examples of polarity of planes with inclination angles in the pink region of Fig. 2(c)). This increases the incorporation coefficients for group V atoms on B polar surfaces and group III atoms on A polar surfaces, reducing their diffusion lengths on the respective facets.

GaAs growth is known to be less sensitive to polarity and form nanowires with regular hexagonal cross-section (or recover this shape after asymmetric growth) [7, 26, 27]. This is due to relatively long diffusion lengths of both, Ga and As [33]. When a considerable percentage of P, which has lower diffusion length than As [25] is added, the average diffusion length of the group V reduces, and this affects the B polar facets more as stated before. As shown in Ref. [6], there will be more group V material laterally flowing out of the {112} A facets due to its lower incorporation rate, leaving an abundance of material in the outside edges of the {112} A facet. The inclined and weakly B polar nanofacets in this region have lower diffusion lengths, blocking this material from migrating too far, and hence, forming the overgrowth. On the alternative vertex, the diffusion away from the {112} B top facet is lower and the diffusion length on the inclined weakly A polar nanofacets remains high enough for the adatoms to diffuse far enough on the {110} facet without accumulating at the corner. This makes the material

deposit closer at the {112} A facet and not so much at the {112} B facets.

In comparison, in the AlGaAs material system, Al has much lower surface diffusion length than Ga [34] and addition of Al (or completely replacing Ga as in AlAs) would reduce the average diffusion length more on the A polar facets where group III atoms form stronger bonds [6]. This results in higher outflow from the {112}B facets and deposition at the vicinity of the same which has weakly A polar inclined facets. This explains the feature formation at opposite polar vertices in current GaAsP nanowire shells [26].

Short diffusion lengths of less than few tens of nanometres that are comparable to the nanowire diameters and facet lengths are necessary to observe these effects. This broadly explains why these are not observed in most previous low P containing GaAsP and low Al containing AlGaAs growths [6, 7]. It may also be the reason for the inclined facet's lack of prominence and definition in the current sample compared to those in the thicker AlAs shells [26] and their simulations [27]. The preference shown in formation of secondary bands in nanowires with relatively larger diameters (within the range observed) (see Fig. S4 in the ESM) may further support the requirement of comparable diffusion and facet lengths for the formation of secondary bands.

2.3 Formation and evolution of multiple segregation bands on the nano-facets

The effect of the above features on a thicker shell of a ternary material, where segregation profiles are able to develop is discussed next in relation to $GaAs_{(1-x)}P_x$.

Figure 3 shows a schematic of a symmetric {112} A vertex of a nanowire core, with approximated planar inclined nanofacets. Due to its convex shape and narrow width, the top {112} A facet presents the highest surface chemical potential compared to the neighbouring facets [1, 2] (see the surface potential diagram in the inset of Fig. 3 and its determination in Section S2 in the ESM). Hence, the adatoms flow outwards as depicted in Fig. 3. As atoms that have longer migration length [25] diffuse better, forming a P rich radial band as discussed before [6]. Adatoms are incident on the inclined nanofacets by diffusion from the {112}A facet and direct impingement (ignoring the axial diffusion which is in the direction perpendicular to that of interest). Of these adatoms, As atoms [25] will diffuse further towards the {110} nanowire facets that have an even lower surface potential, more so than the P atoms; but to a lesser extent than with respect to the top

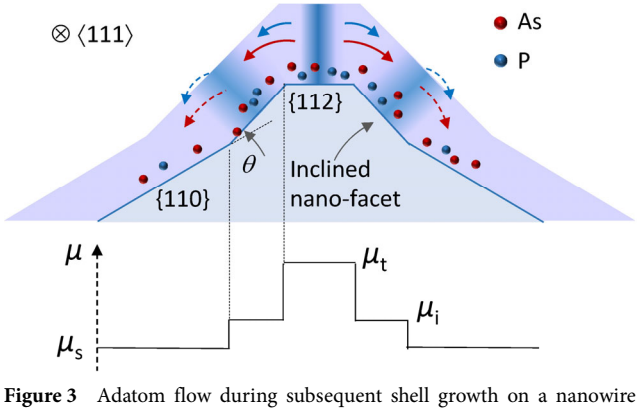

Figure 3 Adatom flow during subsequent shell growth on a nanowire core with inclined facets at the vertices. The shaded regions in the shell indicate the possible segregations of alloys and the inset plots the variation of surface chemical potentials of the facets which are governed by the facet type, size and angles of intersection.

{112} facet, forming less prominent secondary bands compared to the primary band.

The lower level of segregation on the inclined facet is due to two reasons. First is the lower surface potential difference between the inclined and the {110} side facets compared to that between the top and the inclined facets, which mainly arises from the larger width of the inclined facets being more comparable to that of the side facets. Second reason is the already reduced effective available adatom ratio of P/As on the inclined facets that arises from a higher proportion of As atoms diffusing away from the {112} facet being incident on the inclined facet. The multiple segregation bands are somewhat analogous to vertical quantum wire formations in V-grooves on patterned substrates [1, 23, 35], although in reverse order, due to reverse direction of adatom flow. The surface chemical potentials shown in the inset of Fig. 3 are calculated considering only the shape effect. While the shape contributes to the largest component of the surface chemical potential, resulting segregation will give rise to strain and a decrease in entropy of mixing [1]. These will partially counter-act the above effects of shape in the subsequent shell growth, until the equilibrium conditions are reached [1]. See Sections S2 and S3 in the ESM for further details.

Width of the inclined facet have been shown to increase with the thickness of the shell, proportionately to the thickness and the length of the {110} side facet [26]. Hence, another implication here is that the surface chemical potential of the inclined facet decreases with the shell thickness due to its increasing width (see Eq. (S3) in the ESM, Section S2). This means that even if a constant angle, θ is assumed (where in reality this may also vary depending on the composition), the level of segregation will decrease with thickness. The resulting secondary bands would be getting broader and more diffused. On the other hand, width of the top {112} facet is not generally observed to change with the thickness in these GaAsP shells [6, 15]. This would mean that the surface chemical potential of the top facet would remain constant. However, the decrease in chemical potential of the inclined facets would mean that the potential difference between the top facet and the inclined facet would increase leading to more outflow of adatoms (Eq. (S5) in the ESM, Section S2). Hence, in theory, the primary line should get more prominent with shell thickness.

As seen in Fig. 1, the above discussed ideal evolution with thickness is not seen in vertices of all nanowires, due to irregularity in shell shape evolution and alloy fluctuations. Figures 4(a)–4(d) show details of a different cross-section from the same sample and shows one of the nanowires that contained a vertex showing controlled evolution. The bottom vertex in Fig. 4(a) shows the broadening of the two secondary lines with the increasing shell thickness. A guide to eye marking the boundary of the secondary bands is drawn in Fig. 4(b), which is a higher magnification image of the bottom radius. The other two radii of the same polarity as the bottom radius show two bands, of which the secondary bands have been interrupted by alloy fluctuations.

2.4 Splitting of the primary band

The ADF intensity profile taken across the region marked by red arrows in the primary band in Fig. 4(b) is shown in Fig. 4(c). It reveals that, this middle P rich band actually consists of two narrower bands as marked by white arrows in Fig. 4(b) and red arrows in Fig. 4(c). As shown in Fig. 4(d), this splitting of the principal radial line is also seen in some places along B polar radii, but to a lower extent.

While the reason for this splitting is not entirely clear, the

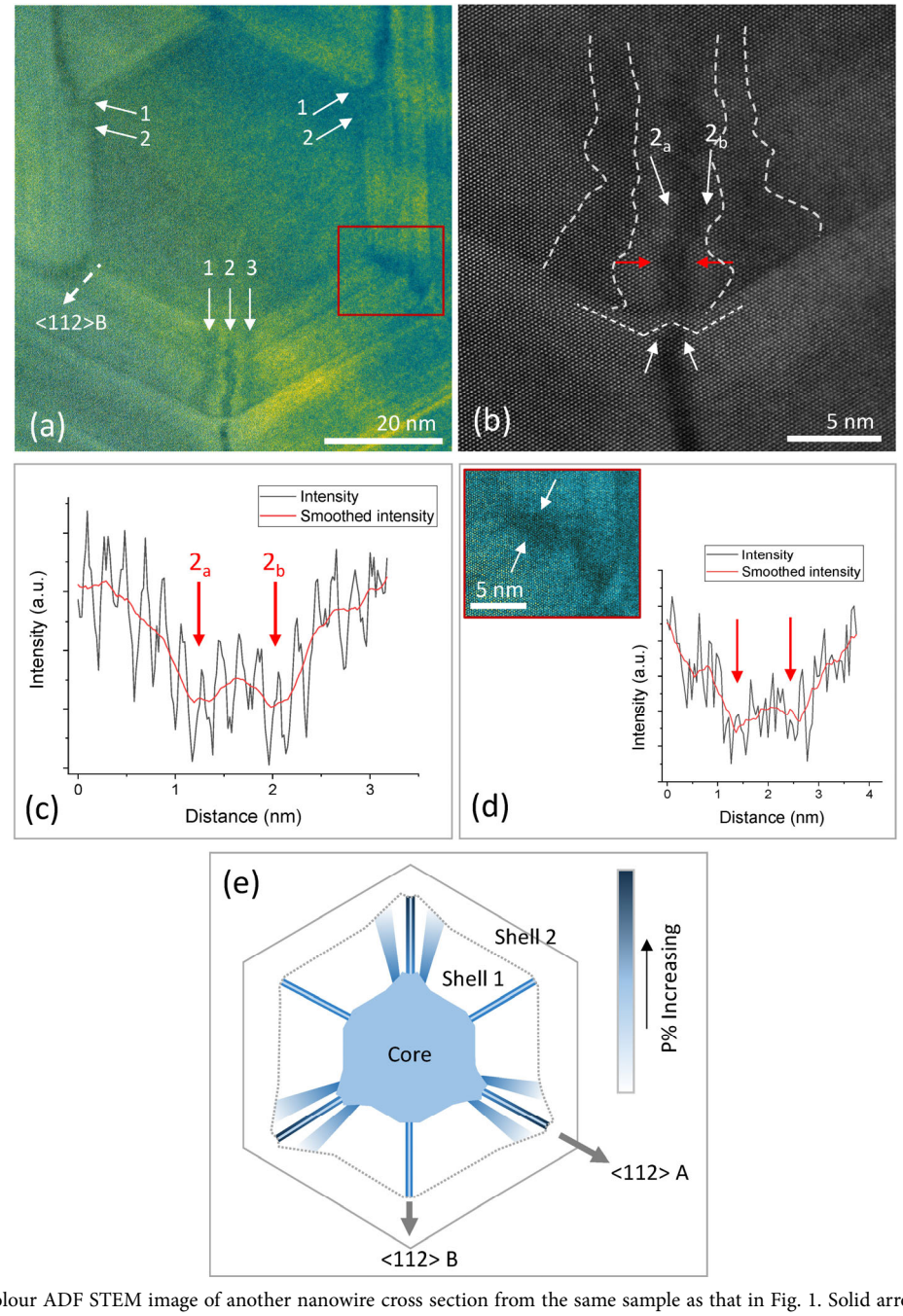

Figure 4 (a) False colour ADF STEM image of another nanowire cross section from the same sample as that in Fig. 1. Solid arrows indicate the P rich bands formed at the <112> A radii. (b) A higher magnification image of the bottom radius in (a), showing the broadening of the secondary bands and two narrow sub-bands that form the primary band. The broken white line is drawn parallel to the interface between the two GaAsP shells. (c) ADF intensity profile across the band at the position marked by the red arrows in (b). Two dips in intensity are present, ~ 1 nm apart. (d) Magnified image of the <112> B radii marked by the red square in (a), showing two faint sub-bands. Inset shows the intensity profile across the position marked by the white arrows. Two dips are seen. (e) Schematic of a nanowire cross section in its most complex form. The <112> A radii would have four P segregation lines and <112> B radii would have two.

sizable {112} facet of the bottom vertex can be roughly seen to be dissociated into two smaller constituent nanofacets, forming a concave shape as shown by the broken-line guides in Fig. 4(b). It has been shown that GaAs {112} facets of both polarities can be unstable and dissociate into surfaces of {110}, {111} and {124} [36, 37]. These dissociated surfaces have lower surface energy than {112} surface, more so under As rich MBE growth conditions similar to those used in the current study [36]. Therefore, here, the total surface related energy at the vertex could be reduced by the dissociation when the {112} facet is sizable, despite creation of an additional concave shape and two sharper vertices. These facets can form a small local surface chemical potential dip in the middle, attracting few As adatoms and splitting the primary P band.

According to the above observations, in its most complex form, the <112> A polar radii in GaAsP shells could contain two secondary P rich bands that fade with thickness and a more prominent primary band which is split in to two sub-bands, while the primary band at the <112> B radii are also split. A schematic summarising this structure and its evolution with shell thickness is given in Fig. 4(e).

2.5 Effect of growth parameters and composition

It was discussed that these secondary lines are sensitive to

alloy fluctuations. Most of them are seen to terminate at alloy fluctuations, while some could even originate at these (Figs. 1(b) and 4(a)). These observations are indicative of their sensitivity to composition of the $GaAs_{(1-x)}P_x$ alloy. As mentioned earlier, when the shell material is an alloy, the effect from shape on the surface chemical potential gets partially regulated by the build-up of strain and reduction of entropy of mixing, both of which arise due to segregation of the alloy (Section S3, Eq. (S6) in the ESM) [1, 8]. This relationship, which incorporates compositions is therefore used to ascertain a relationship between the $GaAs_{(1-x)}P_x$ composition and the formation of the secondary P rich bands.

Regulation of surface chemical potential will result in that of As decreasing on the top and inclined facets, and that of P increasing on both facets (Eqs. (S7)–(S11) in the ESM). In order to continue the adatom flow in the required direction and form multiple P rich bands such that compositions $x_t, x_i > x_s$, the surface chemical potentials for As should be $\mu_{t,A} > \mu_{i,A} > \mu_{s,A}$, and the composition normalised lateral surface fluxes, j_N should be $j_{N,it,A} > j_{N,it,P}$ and $j_{N,si,A} > j_{N,si,P}$ (the splitting of the centre P rich band is not considered in the current growth model, and subscripts t, i, s, A, P refer to the top, inclined and side facets, and As and P, respectively).

Figure 5 plots the maximum possible range of $GaAs_{(1-x)}P_x$ shell composition x_s against small θ values similar to those experimentally observed, where the above inequalities could be satisfied and hence facilitate formation of multiple P rich bands. The shaded areas refer to different r ratios of diffusion coefficients and surface adatom densities of As and P, where $r = (n_{it,si}D_{t,i})_{As}/(n_{it,si}D_{t,i})_P$ (see Eq. (S5) in the ESM). The details of the parameters used for the plot are given in the ESM, Section S3.

Few interesting inferences can be made from this plot. For small values of θ and r, the secondary bands could only form in the high P composition shells. The other indication is that the minimum P composition for the formation of the multiple radial bands reduces with the ratio between the coefficients, r. Although the absolute values may differ due to the actual parameter values under the growth conditions being different to those adopted from literature [38, 39], the trends indicated in Fig. 5 explain the absence of such multiple radial bands in GaAsP shells of lower P composition (< 0.5) that has been studied before [6, 15]. For small angles of θ, the range of shell compositions that allows the formation of multiple radial lines is relatively narrow. When the alloy composition fluctuates to outside of this region, visible secondary radial segregations are interrupted. This justifies their sensitivity to composition and alloy fluctuations within the GaAsP shell.

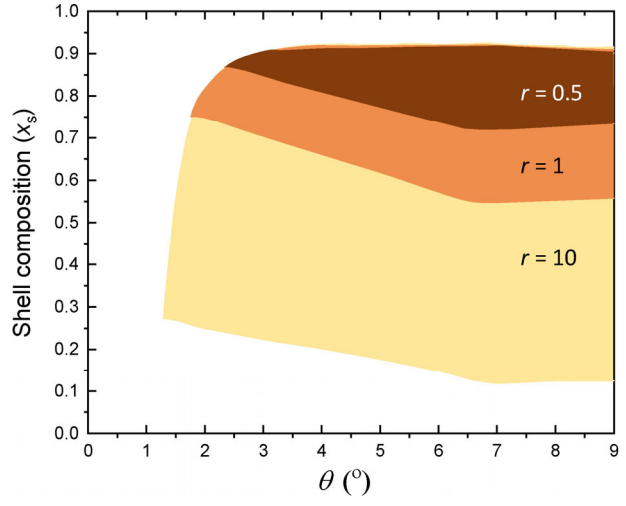

Figure 5 Shell composition x_s ranges where multiple P rich bands can form, plotted against the inclination angle θ. The shaded regions correspond to different $r = (n_{it,si}D_{t,i})_{As} / (n_{it,si}D_{t,i})_P$, As:P surface flux coefficient ratios. Note that the higher r regions encompass the lower r regions.

The multiple P rich bands are not observed in the outer (intentional) shell, albeit having a similar and high composition of P as the inner (unintentional) shell. While one reason could be the higher level of alloy fluctuations, which makes the formation and continuation of the bands difficult, another reason could be the different growth conditions. As elaborated in the experimental section, the inner shell was mainly grown under a higher temperature and low precursor fluxes. These conditions result in the increase in the ratio r, due to the ratio between the sticking coefficients of As and P increasing with temperature [40]. With the increase of the ratio, the minimum P composition for the multiple radial band formation has decreased and the range of allowed compositions increased. Therefore, in this case it appears that the ~ 0.5–0.7 P composition range observed in the current nanowire shells is allowed to form secondary bands only under the high r shell 1 growth conditions and not under those of shell 2, despite their compositions being similar.

It should be noted that the inclination angle θ is considered to be independent in the current model. However, the possibility to maintain angle θ may also depend on the shell composition x_s [27]. This aspect makes the real growth more complex and interdependent, together with the above discussed points, well explaining the difficulty seen in formation and continuation of the secondary P rich bands.

3 Conclusions

Formation of multiple P segregation lines at the radii connecting the vertices of the hexagonal $GaAs_{(1-x)}P_x$ nanowire shells were studied. In its most complex form, the <112> A radii formed four segregation lines, while the <112> B radii formed two. Their formation was found to be a result of two types of nanofacets forming at the vertices of the nanowires, of which, one type only formed at vertices of <112> A polarity. The resulting multiple segregation lines were shown to be driven by the relative migration of As and P adatoms, away from the facets with higher surface chemical potential. The secondary P rich bands at <112> A radii was shown to be evolving with the shell thickness. It was found that a high P composition was necessary for the formation of these bands. In addition, growth conditions that increase the diffusivity difference between As and P were found to increase the likelihood of forming multiple radial lines.

Nanowire QWs are often assembled in the radial and axial directions in tubular and disc forms, respectively [41–44]. The current results demonstrate a self-formation of composition varied finite regions within the nanowire in the form of P deficient radial bands encompassed between P rich bands. As proposed in the introduction, one of the most appealing uses of these formations would be to be engineered as QWs in the circumferential direction, which is both novel and unattainable if not for self-assembly (due to the layer by layer nature of shell growth around the nanowire). Although demonstrated here for GaAsP, this concept can be extended to other ternary compounds such as AlGaAs and InGaAs, where lower band gap binary constituent species have higher diffusion lengths. The understanding of their formation gained through this work can be used to intentionally form designed structures

with desired properties. Grown together with other intentional structures, these circumferential radial QWs can be used to enhance the properties of the former by using them as captors and selective injectors of carriers into the intentionally grown areas, similar to vertical quantum wells and wires in V-grooves and inverted pyramids [23, 24]. Thus, this work paves the way to incorporating quantum wells in nanowires in a novel dimension, which would greatly enhance the versatility of nanowires for complex device designs.

4 Experimental methods

The GaAsP nanowires were grown by solid source molecular beam epitaxy (SSMBE) on Si (111) substrates, using Ga droplet self-catalysed technique. The GaAsP nanowire cores were grown for 90 min at 640 °C with Ga, As and P fluxes of 9.2×10^{-8}, 1.7×10^{-6} and 1.2×10^{-6} Torr, respectively. These growth conditions yielded nanowires of around 10 μm in length. For the core only sample, the growth was terminated immediately after this step. In the core–shell nanowires, the Ga droplet left from the core growth was consumed in two steps of 10 min each before the shell growth. As and P fluxes used for the two steps are 6.8×10^{-7} and 3.5×10^{-7}, and 5.1×10^{-6} and 5.0×10^{-6} Torr, respectively. The 1st shell (shell 1) and the multiple radial bands are formed during these Ga particle consumption steps most likely using the residual Ga left in the chamber. Since the multiple radial bands are more commonly observed closer to the core and the available amount of residual Ga depletes with time, they are presumed to have formed during the first of the two particle consumption steps. The intentional outer shell (shell 2) was grown at a lower temperature of 550 °C for 60 min with Ga, As and P fluxes of 9.2×10^{-8}, 5.1×10^{-6} and 5.0×10^{-6} Torr, respectively.

The nanowire cross-sections were prepared by embedding them in low-viscosity (LV) resin followed by microtome sectioning. The microtome slices were approximately 80 nm thick. The STEM analysis was carried out using a Jeol ARM 200F microscope operating at 200 kV. The EDX compositional analysis was performed using an Oxford Instruments 100 mm^2 windowless detector installed within the same microscope. SEM analysis shown in the ESM was carried out using a Zeiss Gemini 500 operating at 10 kV.

Acknowledgements

This work was supported by the EPSRC grants Nos. EP/P000916/1 and EP/P000886/1. The University of Warwick Electron Microscopy Research Technology Platform and the EPSRC National Epitaxy Facility are acknowledged for providing access to the equipment used. Dr. Anton Velichko is thanked for the careful reading of the manuscript.

The data set related to this publication may be obtained from https://wrap.warwick.ac.uk/140556.

Electronic Supplementary Material: Supplementary material (a scanning electron microscopy image of the examined sample; a schematic showing the relative diffusion of adatoms away from {112} faceted vertices in nanowires during shell growth; surface atoms, bonding arrangements and polarity of some planes that are perpendicular to (111), and parallel to {112} and {110} and form a concave shape with {110}; relationship between the diameter of the nanowires and the formation of multiple segregation bands; derivation of relative surface chemical potentials of the facets at a nano-faceted vertex; calculation of composition range where multiple radial lines can form in $GaAs_{(1-x)}P_x$ nanowires) is available in the online version of this article at https://doi.org/10.1007/s12274-020-3060-x.

References

[1] Biasiol, G.; Gustafsson, A.; Leifer, K.; Kapon, E. Mechanisms of self-ordering in nonplanar epitaxy of semiconductor nanostructures. *Phys. Rev. B* **2002**, *65*, 205306.

[2] Ozdemir, M.; Zangwill, A. Theory of epitaxial growth onto nonplanar substrates. *J. Vac. Sci. Technol. A* **1992**, *10*, 684–690.

[3] Chen, C.; Shehata, S.; Fradin, C.; LaPierre, R.; Couteau, C.; Weihs, G. Self-directed growth of AlGaAs core–shell nanowires for visible light applications. *Nano Lett.* **2007**, *7*, 2584–2589.

[4] Ameruddin, A. S.; Fonseka, H. A.; Caroff, P.; Wong-Leung, J.; het Veld, R. L. O.; Boland, J. L.; Johnston, M. B.; Tan, H. H.; Jagadish, C. $In_xGa_{1-x}As$ nanowires with uniform composition, pure wurtzite crystal phase and taper-free morphology. *Nanotechnology* **2015**, *26*, 205604.

[5] Sköld, N.; Wagner, J. B.; Karlsson, G.; Hernán, T.; Seifert, W.; Pistol, M. E.; Samuelson, L. Phase segregation in AlInP shells on GaAs nanowires. *Nano Lett.* **2006**, *6*, 2743–2747.

[6] Zhang, Y. Y.; Sanchez, A. M.; Wu, J.; Aagesen, M.; Holm, J. V.; Beanland, R.; Ward, T.; Liu, H. Y. Polarity-driven quasi-3-fold composition symmetry of self-catalyzed III–V–V ternary core–shell nanowires. *Nano Lett.* **2015**, *15*, 3128–3133.

[7] Zheng, C. L.; Wong-Leung, J.; Gao, Q.; Tan, H. H.; Jagadish, C.; Etheridge, J. Polarity-driven 3-fold symmetry of GaAs/AlGaAs core multishell nanowires. *Nano Lett.* **2013**, *13*, 3742–3748.

[8] Wagner, J. B.; Sköld, N.; Wallenberg, L. R.; Samuelson, L. Growth and segregation of GaAs–$Al_xIn_{1-x}P$ core-shell nanowires. *J. Cryst. Growth* **2010**, *312*, 1755–1760.

[9] Ng, K. W.; Ko, W. S.; Chen, R.; Lu, F. L.; Tran, T. T. D.; Li, K.; Chang-Hasnain, C. J. Composition homogeneity in InGaAs/GaAs core–shell nanopillars monolithically grown on silicon. *ACS Appl. Mater. Interfaces* **2014**, *6*, 16706–16711.

[10] Yuan, X. M.; Caroff, P.; Wong-Leung, J.; Tan, H. H.; Jagadish, C. Controlling the morphology, composition and crystal structure in gold-seeded $GaAs_{1-x}Sb_x$ nanowires. *Nanoscale* **2015**, *7*, 4995–5003.

[11] Francaviglia, L.; Tütüncüoglu, G.; Martí-Sánchez, S.; Di Russo, E.; Steinvall, S. E.; Ruiz, J. S.; Potts, H.; Friedl, M.; Rigutti, L.; Arbiol, J. et al. Segregation scheme of indium in AlGaInAs nanowire shells. *Phys. Rev. Mater.* **2019**, *3*, 023001.

[12] Rudolph, D.; Funk, S.; Döblinger, M.; Morkötter, S.; Hertenberger, S.; Schweickert, L.; Becker, J.; Matich, S.; Bichler, M.; Spirkoska, D. et al. Spontaneous alloy composition ordering in GaAs-AlGaAs core–shell nanowires. *Nano Lett.* **2013**, *13*, 1522–1527.

[13] Jeon, N.; Loitsch, B.; Morkoetter, S.; Abstreiter, G.; Finley, J.; Krenner, H. J.; Koblmueller, G.; Lauhon, L. J. Alloy fluctuations act as quantum dot-like emitters in GaAs-AlGaAs core–shell nanowires. *ACS Nano* **2015**, *9*, 8335–8343.

[14] Loitsch, B.; Jeon, N.; Döblinger, M.; Winnerl, J.; Parzinger, E.; Matich, S.; Wurstbauer, U.; Riedl, H.; Abstreiter, G.; Finley, J. J. et al.

Suppression of alloy fluctuations in GaAs-AlGaAs core-shell nanowires. *Appl. Phys. Lett.* **2016**, *109*, 093105.
[15] Fonseka, H. A.; Velichko, A. V.; Zhang, Y. Y.; Gott, J. A.; Davis, G. D.; Beanland, R.; Liu, H. Y.; Mowbray, D. J.; Sanchez, A. M. Self-formed quantum wires and dots in GaAsP-GaAsP core-shell nanowires. *Nano Lett.* **2019**, *19*, 4158–4165.
[16] Arbiol, J.; Magen, C.; Becker, P.; Jacopin, G.; Chernikov, A.; Schäfer, S.; Furtmayr, F.; Tchernycheva, M.; Rigutti, L.; Teubert, J. et al. Self-assembled GaN quantum wires on GaN/AlN nanowire templates. *Nanoscale* **2012**, *4*, 7517–7524.
[17] Schmidt, G.; Müller, M.; Veit, P.; Metzner, S.; Bertram, F.; Hartmann, J.; Zhou, H.; Wehmann, H. H.; Waag, A.; Christen, J. Direct imaging of Indium-rich triangular nanoprisms self-organized formed at the edges of InGaN/GaN core-shell nanorods. *Sci. Rep.* **2018**, *8*, 16026.
[18] Heiss, M.; Fontana, Y.; Gustafsson, A.; Wüst, G.; Magen, C.; O'Regan, D. D.; Luo, J. W.; Ketterer, B.; Conesa-Boj, S.; Kuhlmann, A. V. et al. Self-assembled quantum dots in a nanowire system for quantum photonics. *Nat. Mater.* **2013**, *12*, 439–444.
[19] Yu, Y.; Dou, X. M.; Wei, B.; Zha, G. W.; Shang, X. J.; Wang, L.; Su, D.; Xu, J. X.; Wang, H. Y.; Ni, H. Q. et al. Self-assembled quantum dot structures in a hexagonal nanowire for quantum photonics. *Adv. Mater.* **2014**, *26*, 2710–2717.
[20] Lähnemann, J.; Hill, M. O.; Herranz, J.; Marquardt, O.; Gao, G. H.; Al Hassan, A.; Davtyan, A.; Hruszkewycz, S. O.; Holt, M. V.; Huang, C. Y. et al. Correlated nanoscale analysis of the emission from wurtzite versus zincblende (In, Ga)As/GaAs nanowire core–shell quantum wells. *Nano Lett.* **2019**, *19*, 4448–4457.
[21] Corfdir, P.; Lewis, R. B.; Marquardt, O.; Küpers, H.; Grandal, J.; Dimakis, E.; Trampert, A.; Geelhaar, L.; Brandt, O.; Phillips, R. T. Exciton recombination at crystal-phase quantum rings in GaAs/$In_xGa_{1-x}As$ core/multishell nanowires. *Appl. Phys. Lett.* **2016**, *109*, 082107.
[22] Ariga, K.; Nishikawa, M.; Mori, T.; Takeya, J.; Shrestha, L. K.; Hill, J. P. Self-assembly as a key player for materials nanoarchitectonics. *Sci. Technol. Adv. Mater.* **2019**, *20*, 51–95.
[23] Weman, H.; Martinet, E.; Rudra, A.; Kapon, E. Selective carrier injection into V-groove quantum wires. *Appl. Phys. Lett.* **1998**, *73*, 2959–2961.
[24] Zhu, Q.; Pelucchi, E.; Dalessi, S.; Leifer, K.; Dupertuis, M. A.; Kapon, E. Alloy segregation, quantum confinement, and carrier capture in self-ordered pyramidal quantum wires. *Nano Lett.* **2006**, *6*, 1036–1041.
[25] Wu, S. D.; Guo, L. W.; Wang, W. X.; Li, Z. H.; Niu, P. J.; Huang, Q.; Zhou, J. M. Incorporation behaviour of arsenic and phosphorus in GaAsP/GaAs grown by solid source molecular beam epitaxy with a GaP decomposition source. *Chin. Phys. Lett.* **2005**, *22*, 960–962.
[26] Jeon, N.; Ruhstorfer, D.; Döblinger, M.; Matich, S.; Loitsch, B.; Koblmüller, G.; Lauhon, L. Connecting composition-driven faceting with facet-driven composition modulation in GaAs–AlGaAs core–shell nanowires. *Nano Lett.* **2018**, *18*, 5179–5185.
[27] Bergamaschini, R.; Montalenti, F.; Miglio, L. Sunburst pattern by kinetic segregation in core-shell nanowires: A phase-field study. *Appl. Surf. Sci.* **2020**, *517*, 146056.
[28] Sato, T.; Tamai, I.; Hasegawa, H. Growth kinetics and modeling of selective molecular beam epitaxial growth of GaAs ridge quantum wires on pre-patterned nonplanar substrates. *J. Vac. Sci. Technol. B* **2004**, *22*, 2266–2274.
[29] Stiles, K.; Kahn, A. Low energy electron diffraction study of (221) and (311) GaAs surfaces. *J. Vac. Sci. Technol. B* **1985**, *3*, 1089–1092.
[30] Jacobi, K.; Geelhaar, L.; Márquez, J. Structure of high-index GaAs surfaces—The discovery of the stable GaAs (2511) surface. *Appl. Phys. A* **2002**, *75*, 113–127.
[31] Chadi, D. J. Atomic and electronic structures of (111), (211), and (311) surfaces of GaAs. *J. Vac. Sci. Technol. B* **1985**, *3*, 1167–1169.
[32] Márquez, J.; Kratzer, P.; Geelhaar, L.; Jacobi, K.; Scheffler, M. Atomic structure of the stoichiometric GaAs(114) surface. *Phys. Rev. Lett.* **2001**, *86*, 115–118.
[33] Palma, A.; Semprini, E.; Talamo, A.; Tomassini, N. Diffusion constant of Ga, In and As adatoms on GaAs (001) surface: Molecular dynamics calculations. *Mater. Sci. Eng. B* **1996**, *37*, 135–138.
[34] Tanaka, M.; Suzuki, T.; Nishinaga, T. Surface diffusion of Al and Ga atoms on GaAs (001) and (111) B vicinal surfaces in molecular beam epitaxy. *J. Crystal Growth* **1991**, *111*, 168–172.
[35] Biasiol, G.; Reinhardt, F.; Gustafsson, A.; Kapon, E. Self-limiting OMCVD growth of GaAs on V-grooved substrates with application to InGaAs/GaAs quantum wires. *J. Electron. Mater.* **1997**, *26*, 1194–1198.
[36] Platen, J.; Kley, A.; Setzer, C.; Jacobi, K.; Ruggerone, P.; Scheffler, M. The importance of high-index surfaces for the morphology of GaAs quantum dots. *J. Appl. Phys.* **1999**, *85*, 3597–3601.
[37] Nötzel, R.; Däweritz, L.; Ploog, K. Topography of high- and low-index GaAs surfaces. *Phys. Rev. B* **1992**, *46*, 4736–4743.
[38] Sibirev, N. V.; Timofeeva, M. A.; Bol'shakov, A. D.; Nazarenko, M. V.; Dubrovskiĭ, V. G. Surface energy and crystal structure of nanowhiskers of III–V semiconductor compounds. *Phys. Solid State* **2010**, *52*, 1531–1538.
[39] http://www.ioffe.rssi.ru/SVA/NSM/Semicond/ (accessed Jan 4, 2020).
[40] Matsushima, Y.; Gonda, S. I. Molecular beam epitaxy of GaP and $GaAs_{1-x}P_x$. *Jpn. J. Appl. Phys.* **1976**, *15*, 2093.
[41] Fonseka, H. A.; Ameruddin, A. S.; Caroff, P.; Tedeschi, D.; De Luca, M.; Mura, F.; Guo, Y.; Lysevych, M.; Wang, F.; Tan, H. H. et al. InP–$In_xGa_{1-x}As$ core-multi-shell nanowire quantum wells with tunable emission in the 1.3–1.55 μm wavelength range. *Nanoscale* **2017**, *9*, 13554–13562.
[42] De la Mata, M.; Zhou, X.; Furtmayr, F.; Teubert, J.; Gradečak, S.; Eickhoff, M.; Fontcuberta i Morral, A.; Arbiol, J. A review of MBE grown 0D, 1D and 2D quantum structures in a nanowire. *J. Mater. Chem. C* **2013**, *1*, 4300–4312.
[43] Qian, F.; Li, Y.; Gradečak, S.; Park, H. G.; Dong, Y. J.; Ding, Y.; Wang, Z. L.; Lieber, C. M. Multi-quantum-well nanowire heterostructures for wavelength-controlled lasers. *Nat. Mater.* **2008**, *7*, 701–706.
[44] Karimi, M.; Jain, V.; Heurlin, M.; Nowzari, A.; Hussain, L.; Lindgren, D.; Stehr, J. E.; Buyanova, I. A.; Gustafsson, A.; Samuelson, L. et al. Room-temperature InP/InAsP quantum discs-in-nanowire infrared photodetectors. *Nano Lett.* **2017**, *17*, 3356–3362.